Conjugated, Rigidified Bibenzimidazole Ancillary Ligands for Enhanced Photoluminescence Quantum Yields of Orange/Red-Emitting Iridium(III) Complexes

*Adam F. Henwood,[a‡] Daniel Antón-García,[a‡] Mégane Morin,[a] Diego Rota Martir,[a] David B. Cordes,[a] Colin Casey,[a] Alexandra M. Z. Slawin,[a] Tomas Lebl,[a] Michael Bühl,[a] and Eli Zysman-Colman[a]**

[a] Organic Semiconductor Centre, EaStCHEM School of Chemistry, University of St Andrews, St Andrews, Fife, KY16 9ST, UK, Fax: +44-1334 463808; Tel: +44-1334 463826;
E-mail: eli.zysman-colman@st-andrews.ac.uk;
URL: http://www.zysman-colman.com

‡ These authors contributed equally

Abstract. A series of six novel $[Ir(C^N)_2(N^N)](PF_6)$ complexes (C^N is one of two cyclometalating ligands: 2-phenyl-4-(2,4,6-trimethylphenyl)pyridine, MesppyH, or 2-(napthalen-1-yl)-4-(2,4,6-trimethylphenyl)pyridine, MesnpyH; N^N denotes one of four neutral diamine ligands: 4,4'-di-*tert*-butyl-2,2'-bipyridine, dtbubpy, 1*H*,1'*H*-2,2'-bibenzimiazole, H_2bibenz, 1,1'-(α,α'-*o*-xylylene)-2,2'-bibenzimidazole, *o*-Xylbibenz or 2,2'-biquinoline, biq) were synthesised and their structural, electrochemical and photophysical properties comprehensively characterised. The more conjugated MesnpyH ligands confer a red-shift in the emission compared to MesppyH but maintain high photoluminescence quantum yields due to the steric bulk of the mesityl groups. The H_2bibenz and *o*-Xylbibenz ligands are

shown to be electronically indistinct to dtbubpy but give complexes with higher quantum yields than analogous complexes bearing dtbubpy. In particular, the rigidity of the *o*-Xylbibenz ligand, combined with the steric bulk of the MesnpyH C^N ligands, give a red-emitting complex **4** (λ_{PL} = 586, 623 nm) with a very high photoluminescence quantum yield (Φ_{PL} = 44%) for an emitter in that regime of the visible spectrum. These results suggest that employing these ligands is a viable strategy for designing more efficient orange-red emitters for use in a variety of photophysical applications.

Introduction.

Phosphorescent emission of transition metal complexes, such as those of Ir(III),[1] Ru(II),[2] and Os(II)[3] complexes, among others, has been a widely studied phenomenon in part because of the plethora of applications that are underpinned by this, but also because of the fundamental interest of chemists in studying molecules that emit light. Indeed, it is often such fundamental studies that inform the eventual applications of these complexes. Among the biggest challenges that remain for photoactive Ir(III) complexes are optimizing the photophysical properties of analogs that can emit in either the deep blue or deep red/near IR regions of the electromagnetic spectrum.

For blue emitters, efficient quenching mechanisms begin to dominate as the HOMO-LUMO energy gap becomes large due to thermal population of non-emissive triplet metal centred (^{3}MC) states,[4] which leads to much a larger non-radiative rate constant (k_{nr}). In addition, the excited states of blue-emitting iridium(III) complexes tend to be ligand centred (LC) in nature, and thus they phosphoresce with a relatively attenuated spin-orbit coupling (SOC) mechanism, resulting in smaller radiative rate constants (k_r) than complexes that emit from a triplet metal-to-ligand charge transfer (^{3}MLCT) state. Failure to largely overcome this problem for blue emitters has limited the power efficiency of electroluminescent devices such as organic light-

emitting diodes (OLEDs)[5] and light-emitting electrochemical cells (LEECs)[6] based on these materials.

For red emitters, the energy gap law becomes increasingly problematic,[7] due to the inverse relationship between the non-radiative rate constant (k_{nr}) and emission energy,[8] and the cubic dependence on the emission energy of the radiative rate constant (k_r).[8-9] Thus, in the case of low energy emitters there is expected to be a simultaneous decrease in k_r and increase in k_{nr}. In particular, the enhancement in k_{nr} is facilitated by progressively more probable Franck-Condon coupling of T_1 vibrational modes with high lying S_0 vibrational modes.[10] Thus, red-emitting OLEDs do not show the same level of efficiencies as green and yellow devices.[11] In addition to devices, red emitters are highly desirable for use in biological applications such as bioimaging[12] and photodynamic therapy,[13] due to the high transmittance of red/IR photons through biological media. Thus, there is considerable interest in developing red-emitting complexes with high quantum yields.

Recently, our group has explored design strategies to achieve high photoluminescence quantum yields (Φ_{PL}) for cationic Ir(III) complexes of the form $[Ir(C^N)_2(N^N)]^+$ (C^N here denotes a bidentate anionic cyclometalating ligand exemplified by the 2-phenylpyridine, ppyH, ligand while N^N is a neutral bidentate diimine ligand such as 2,2'-bipyridine, bpy). We have particularly focussed on addressing the aforementioned challenges related to blue emitters,[14] and have demonstrated that a combination of rigid and sterically bulky ligand chelates effectively suppress *intra*- and *inter*molecular contributions to the non-radiative rate constant (k_{nr}), leading to Φ_{PL} values of blue- and green-emitting cationic $[Ir(C^N)_2(N^N)]^+$ complexes in both MeCN solution and doped thin films that approach unity. Specifically, we found that replacing the prototypical N^N ligand 4,4'-di-*tert*-butyl-2,2'-bipyridine (dtbubpy) with a

modified biimidazole N^N ligand containing a rigid tethering unit (1,1'-(α,α'-*o*-xylylene)-2,2'-biimidazole, *o*-Xylbiim) restricted conformational motion of the chelate in both the ground and excited states, suppressing these deleterious intramolecular non-radiative decay pathways.[14e] The rational ancillary ligand design was combined with modification of an archetypal C^N ligand (2,4-difluorophenylpyridine, dFppyH) with a bulkier analogue (2-(2,4-difluorophenyl)-4-mesitylpyridine, dFMesppy) to suppress intermolecular quenching, leading to a photoluminescence quantum yield of 90% in MeCN solution (Chart 1).[14h]

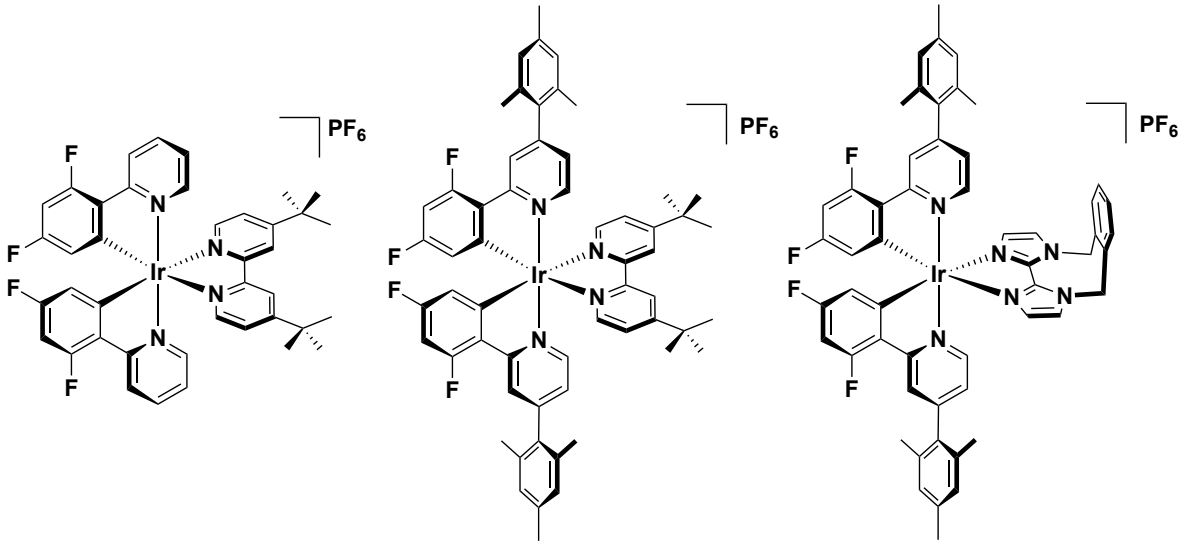

λ_{PL} (nm) =	515	515	459, 487
Φ_{PL} (%) =	72	80	90
Name:	[Ir(dFppy)$_2$(dtbubpy)](PF$_6$)	[Ir(dFMesppy)$_2$(dtbubpy)](PF$_6$)	[Ir(dFMesppy)$_2$(*o*-Xylbiim)](PF$_6$)

Chart **1**. Previously studied complexes modified to achieve high photoluminescence quantum yields.[14h]

Given the efficacy of the *o*-Xylbiim ligand in reducing vibrational contributions to k_{nr} for blue emitters, we thus considered whether this rigid ligand motif could be employed as a universal design strategy for emitters across the visible spectrum. In particular, we wished to see if this could be applied to suppressing the coupling of the excited state to non-emissive Franck-Condon vibronic modes that quench the emission of red-emitters.

Several strategies[4] can be employed to red-shift the emission in cationic iridium complexes, which include (but are not limited to): (1) destabilising the energy of the HOMO (typically localised on the metal and C^N ligands) and/or stabilising the energy of the LUMO (typically localised on the N^N ligands) with appropriate electron-donating[15] and/or accepting[16] functionalities; (2) inducing excimer-based emission;[11b] (3) extending the effective conjugation length of the ligands.[17] In this study, we explore conjugated analogues of our previously reported biimidazole ligands: 1*H*,1'*H*-2,2'-bibenzimiazole (H_2bibenz) and its xylylated derivative (1,1'-(α,α'-*o*-xylylene)-2,2'-bibenzimidazole, *o*-Xylbibenz). The extended conjugation present in the bibenzimidazole core was expected to promote a red-shifted emission compared to the previously studied biimidazole complexes, while it was anticipated that application of our rigid tethering strategy here would effectively mitigate contributions to k_{nr}, thereby leading to emitters showing higher Φ_{PL}.

To evaluate this emitter design, six new cationic iridium complexes were synthesized (Chart **2**). Complexes **1** and **2** utilise our previously reported 2-phenyl-4-(2,4,6-trimethylphenyl)pyridine (MesppyH) C^N ligand.[18] Cationic iridium complexes bearing bulky ligands have been explored in the literature,[19] and indeed this ligand, and fluorinated analogues bearing the mesityl group installed at the 4-position of the coordinating pyridine ring,[14h, 14m, 20] have been shown to be effective at improving: (1) the solubility of the complex in organic solvents such as DCM and MeCN, which is important for producing films with a homogeneous morphology in the solution-processed devices; and (2) impeding intermolecular processes from occurring resulting in diminished non-radiative decay as a function of the steric bulk of the mesityl rings. Complexes **1** and **2** differ in the nature of the bibenzimidazole ligand. For **1**, the distal nitrogen atoms are protonated (H_2bibenz) while for **2** there is the xylylene tether (*o*-Xylbibenz). Complexes **3** and **4** possess a more conjugated C^N ligand (2-(napthalen-1-yl)-4-

(2,4,6-trimethylphenyl)pyridine, MesnpyH) in order to promote a further red-shift in the emission as a function of HOMO destabilization. In addition to these four complexes, we have also synthesized two reference complexes employing the MesnpyH C^N ligand: complex **5**, which contains the much employed 4,4'-di-*tert*-butyl-2,2'-bipyridine (dtbubpy) N^N ligand and complex **6**, employing the highly conjugated 2,2'-biquinoline (biq) ligand, which had previously been used to produce deep red-emitting cationic iridium complexes in combination with C^N ligands such as ppyH[21] and 1-phenylpyrazole (ppzH).[22]

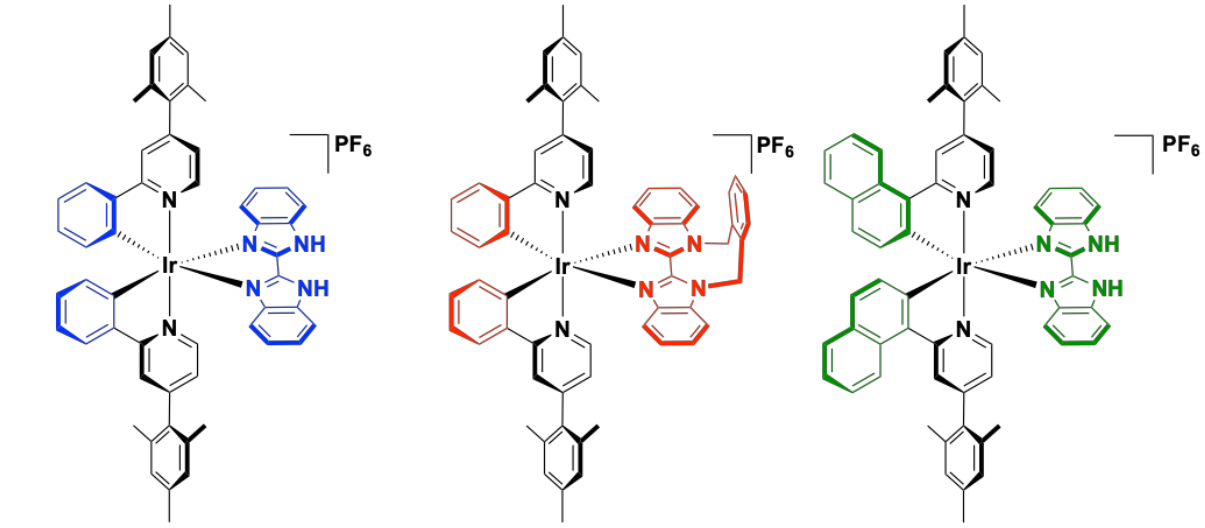

Number: 1 **Name:** [Ir(Mesppy)$_2$(H$_2$bibenz)](PF$_6$)

2 [Ir(Mesppy)$_2$(*o*-Xylbibenz)](PF$_6$)

3 [Ir(Mesnpy)$_2$(H$_2$bibenz)](PF$_6$)

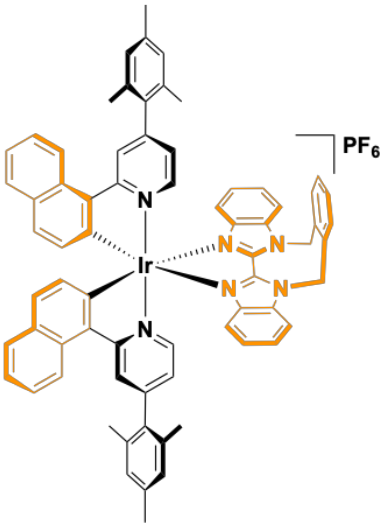

Number: 4 **Name:** [Ir(Mesnpy)$_2$(*o*-Xylbibenz)](PF$_6$)

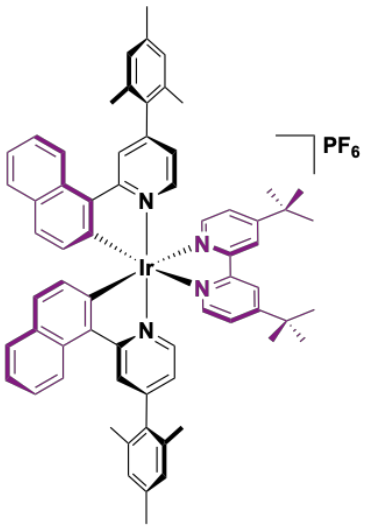

5 [Ir(Mesnpy)$_2$(dtbubpy)](PF$_6$)

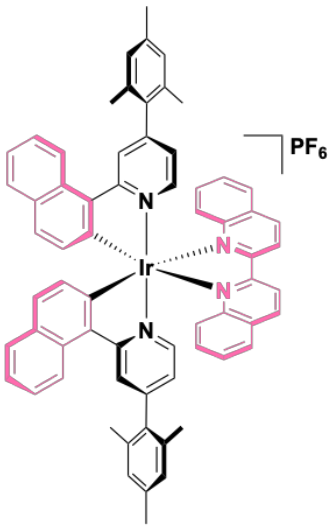

6 [Ir(Mesnpy)$_2$(biq)](PF$_6$)

Chart **2**. Complexes reported in this study.

Results and Discussion.

Synthesis.

The ligand syntheses are outlined in Scheme **1**. The N^N ligand H_2bibenz was synthesised in two steps in excellent yield from *o*-nitroaniline, which was first reduced using $SnCl_2$ to give the diamine (95%) and subsequently condensed with 2,2,2,-trichloroacetimidate (92%).[23] *o*-Xylbibenz was obtained in good yield by alkylation of H_2bibenz with α,α'-dibromo-*o*-xylene in MeCN (60%), under analogous conditions to our previous report.[14e] The C^N ligands were obtained through a sequential set of Suzuki-Miyaura cross-coupling reactions using a previously reported strategy (MesppyH = 96% and MesnpyH = 68%).[18b, 18c]

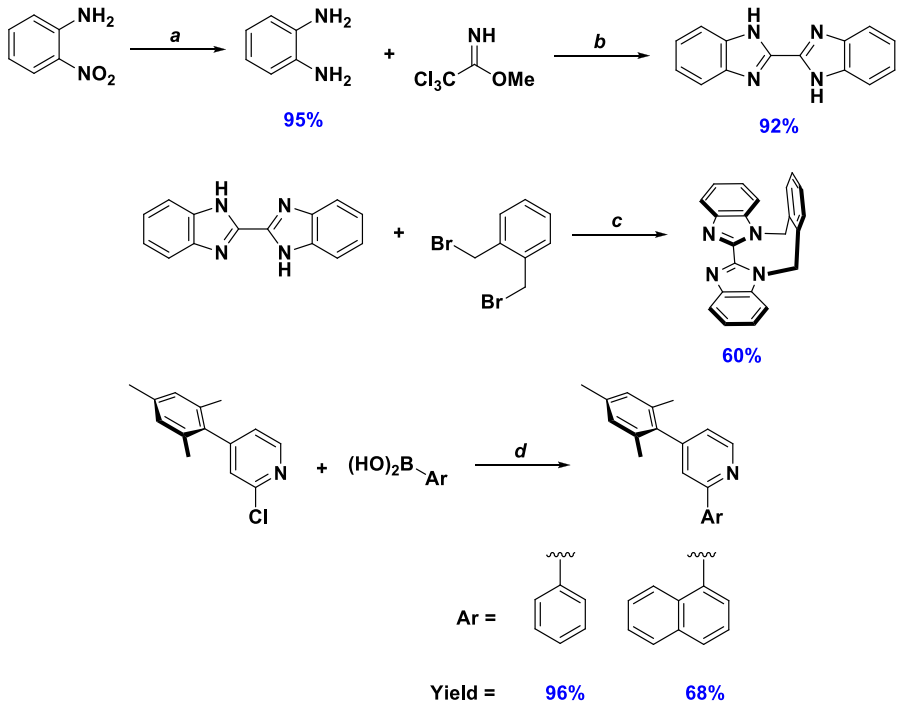

Scheme **1**. Synthesis of organic intermediates and ligands. [a] $SnCl_2$ (3.6 equiv.), EtOH, HCl, 60 °C, 16 h, N_2. [b] i) MeOH, HCl, 0 °C, 3 h, N_2 ii) K_2CO_3 (1.0 equiv.), rt, 39 h, N_2. [c] MeCN, $NaOH_{(aq)}$ (5.6 equiv.), 80 °C, 19 h, N_2. [d] $Pd(PPh_3)_4$ (5 mol%), K_2CO_3 (2.8 equiv.), 1,4-dioxane/water (3:1 v/v), 100 °C, 19 h, N_2.

The intermediate dichloro-bridged iridium dimers were synthesised using $IrCl_3.3H_2O$ in the presence of excess C^N ligand in a refluxing mixture of 2-ethoxyethanol and water.[24] The mononuclear iridium complexes were obtained by cleaving the $[Ir(C^N_2)(\mu\text{-}Cl)]_2$ dimer with a small excess of N^N ligand in a refluxing solution of DCM/MeOH. Purification was carried out first by silica gel chromatography, then anion metathesis was achieved by precipitating concentrated MeOH solutions of the complexes from aqueous NH_4PF_6 solutions. The compounds were then recrystallised. Scheme **2** summarises reagents and conditions employed in the synthesis of complexes **1**–**6**.

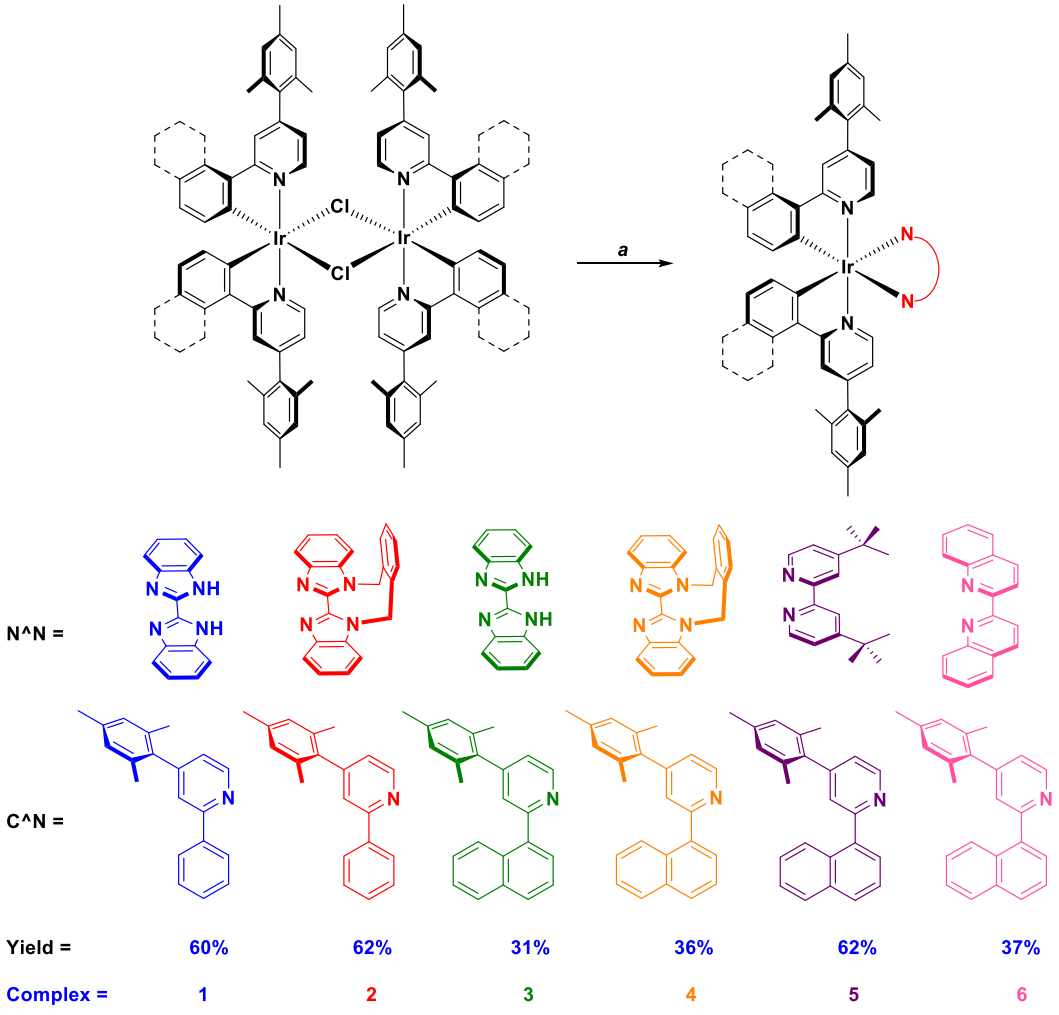

Scheme **2**. Synthesis of **1**–**6**. Reagents and conditions: [a] N^N ligand (2.2 equiv.), CH_2Cl_2/MeOH (1:1 v/v), reflux, 24 h, N_2.

Chemical and Structural Characterization.

All complexes, as well as the new C^N ligand MesnpyH, were fully characterised by ^1H and ^{13}C NMR spectroscopy, high-resolution mass spectrometry (HRMS), melting point analysis, and elemental analysis (EA). Finally, the structure of the MesnpyH C^N ligand, as well as the structures of complexes **1** and **3**–**6** were unequivocally determined by single crystal X-ray diffraction analysis.

Previous studies on [Ir(dFppy)$_2$(*o*-Xylbiim)](PF$_6$) and [Ir(dFMesppy)$_2$(*o*-Xylbiim)](PF$_6$) displayed broad and featureless ^1H NMR spectra, and additional signals indicative of multiple conformers in solution. The complexity of these ^1H NMR spectra was attributed to diastereomeric atropisomerism, a consequence of the slow inversion kinetics of the *o*-Xylbiim between its two conformations, as well as slow rotation of the mesityl ring with respect to the pyridine in the case of [Ir(dFMesppy)$_2$(*o*-Xylbiim)](PF$_6$), coupled with the stereochemistry at iridium. Complex **2** (Figure **1**), bearing the *o*-Xylbibenz ligand, shows a ^1H NMR spectrum with relatively sharper signals at room temperature compared to complexes possessing the *o*-Xylbiim ligand. However, very broad signals are apparent at around 6.3 and 6.9 ppm associated with the methylene resonances associated with the tethered xylylene in the *o*-Xylbibenz ligand, which indicate that conformational exchange is again slow on the NMR time scale. To better understand the conformational dynamics, the sample was heated in solutions of DMSO-d_6 to 372 K. Sharpening of broad signals with increasing temperature was observed and the AB spin system pattern of the methylene protons within the *o*-Xylbibenz ligand methylene group was

revealed in the region around 6.3 ppm. Therefore, we assume that the restricted dynamic is likely associated with the ring flipping between the two *o*-Xylbibenz conformations analogous to the one already described for complexes with the *o*-Xylbiim ligand.[14e, 14h] A similar assumption could be also made for complex **4** since, although the AB spin system pattern is less apparent, restricted conformational exchange affects signals in the same chemical shift regions (Figure **2**).

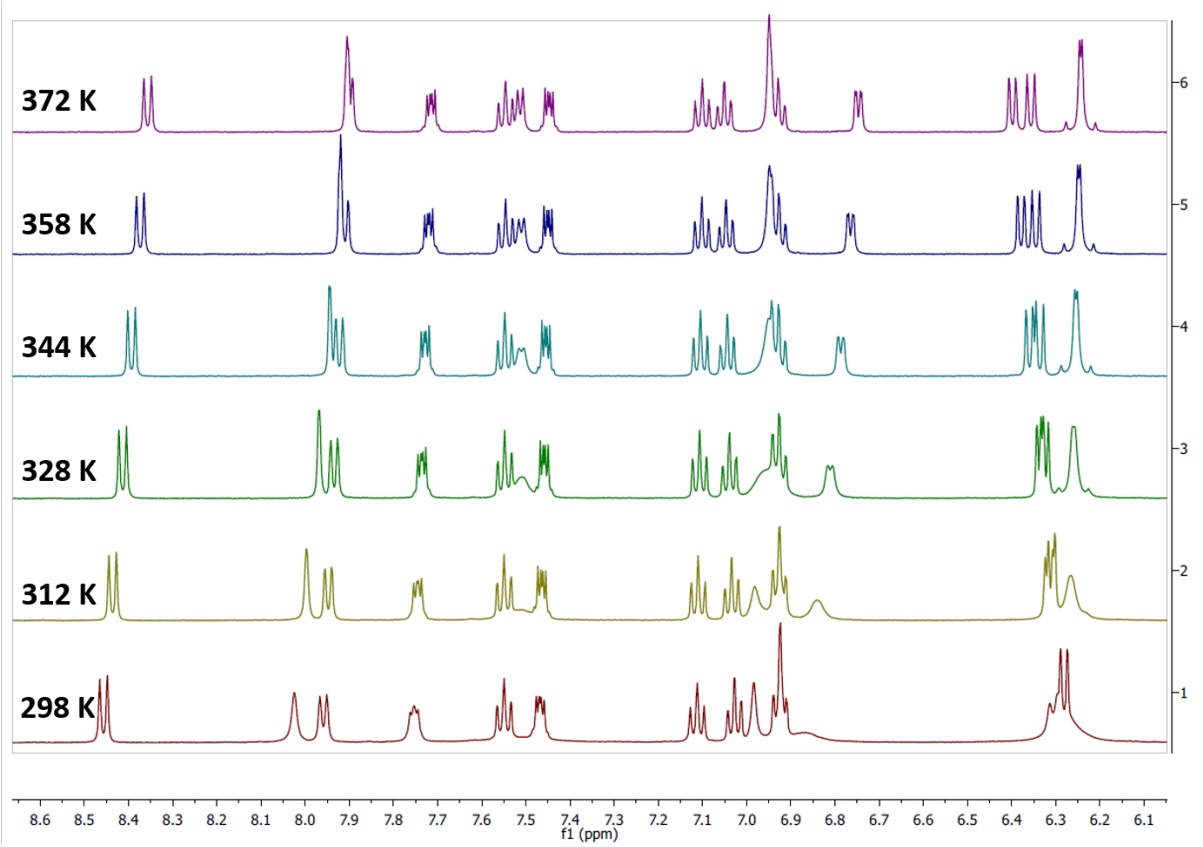

Figure **1**. ^{1}H NMR temperature study of complex **2** in DMSO-d_6.

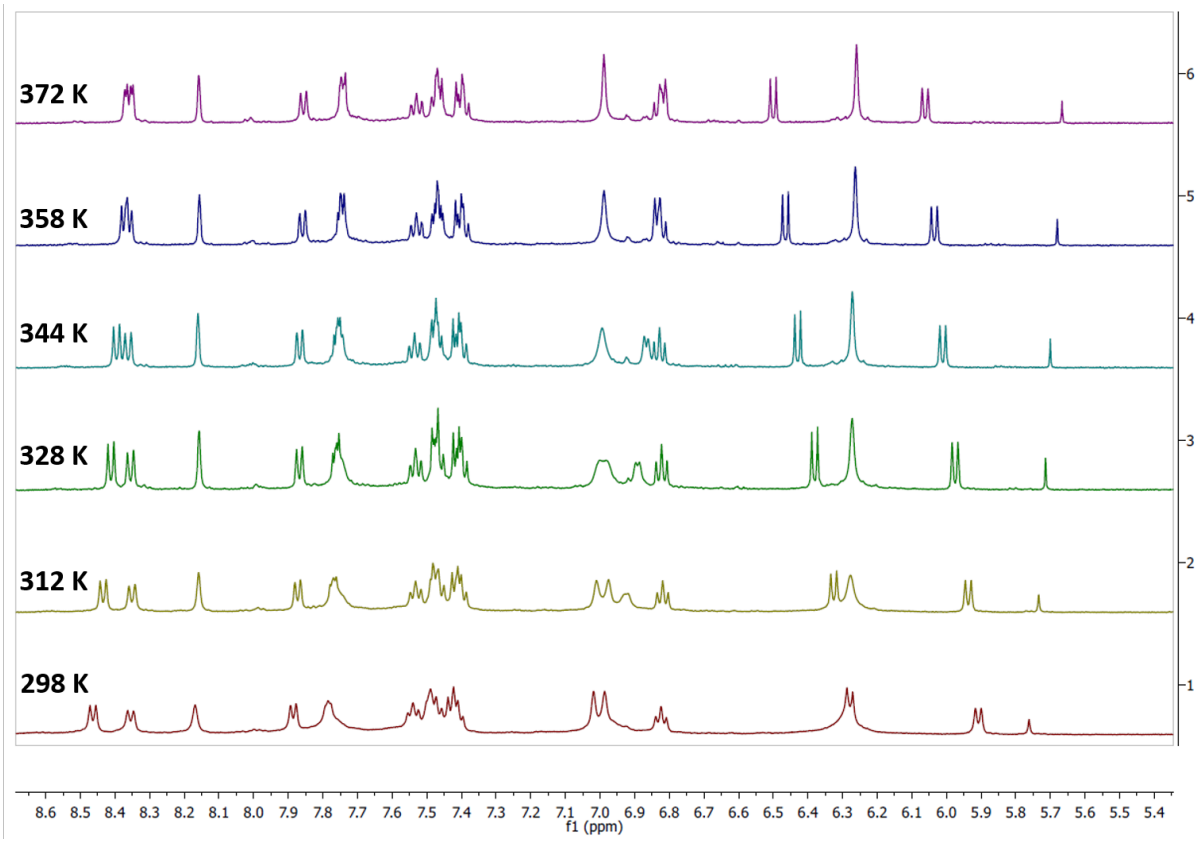

Figure **2**. ^{1}H NMR temperature study of complex **4** in DMSO-d_6.

In contrast to the C^N ligands dFMesppy and Mesppy, which are viscous oils at room temperature, Mesnpy forms white crystals upon cooling, facilitated by π-π stacking of adjacent naphthalene rings (Figure **5**), at centroid-to-centroid distances of 3.6146(11) and 3.7689(11) Å. As expected, the methyl groups on the mesityl ring induce a large torsional angle between the mesityl and pyridine rings [79.60(19)^{o}]. Steric effects also induce a significant [43.2(2)^{o}] torsional twist between the naphthalene and the pyridine rings.

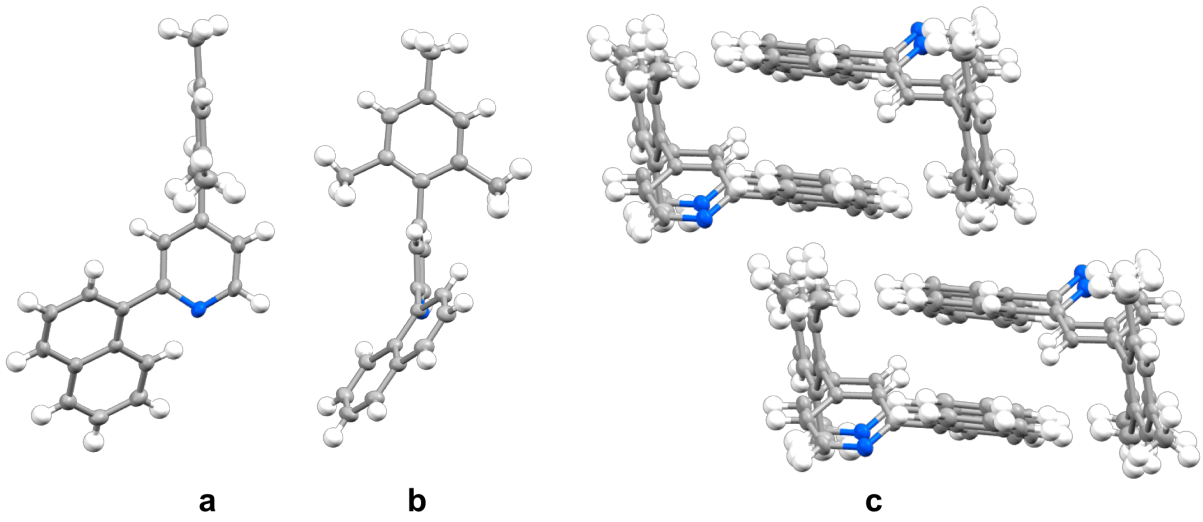

Figure **5**. X-ray crystal structures of Mesnpy viewed facing the pyridine (a) and the mesityl (b). Packing of Mesnpy (c) showing packing of adjacent dimers.

The crystal structures of **1** and **3**–**6** show the expected distorted octahedral geometries with the pyridyl nitrogen atoms of the C^N ligands in the usual *trans* configuration (Figure **6**). Complexes **1** [H···F distances 1.875 – 2.157 Å, and corresponding N···F distances 2.81(2) – 3.00(4) Å] and **3** [H···F distances 1.98(3) and 2.08(6) Å, and corresponding N···F distances 2.858(5) and 2.949(6) Å] form tight hydrogen bonds between the -NH hydrogen atoms and the PF_6^- counteranion, similar to other complexes featuring H_2biim[14e, 25] and H_2bibenz ligands.[26] All five structures show the mesityl groups adopting a highly twisted conformation with respect to the pyridine ring [torsions 66.1(4) – 86.2(3)°]. Furthermore, the distortion of the naphthalene ring with respect to the pyridine observed in the crystal structure of Mesnpy is also observed in the structures of **3**–**6**. While there is essentially no torsional twist between the phenyl and pyridine rings of Mesppy in **1** [0(2) – 3(2)°], the analogous torsional distortions between phenyl and naphthyl rings of Mesnpy are all significantly larger for **3**–**6** [15.1(4) – 31.0(4)°], which is a result of the naphthalene rings minimising steric interactions with the pyridine rings.

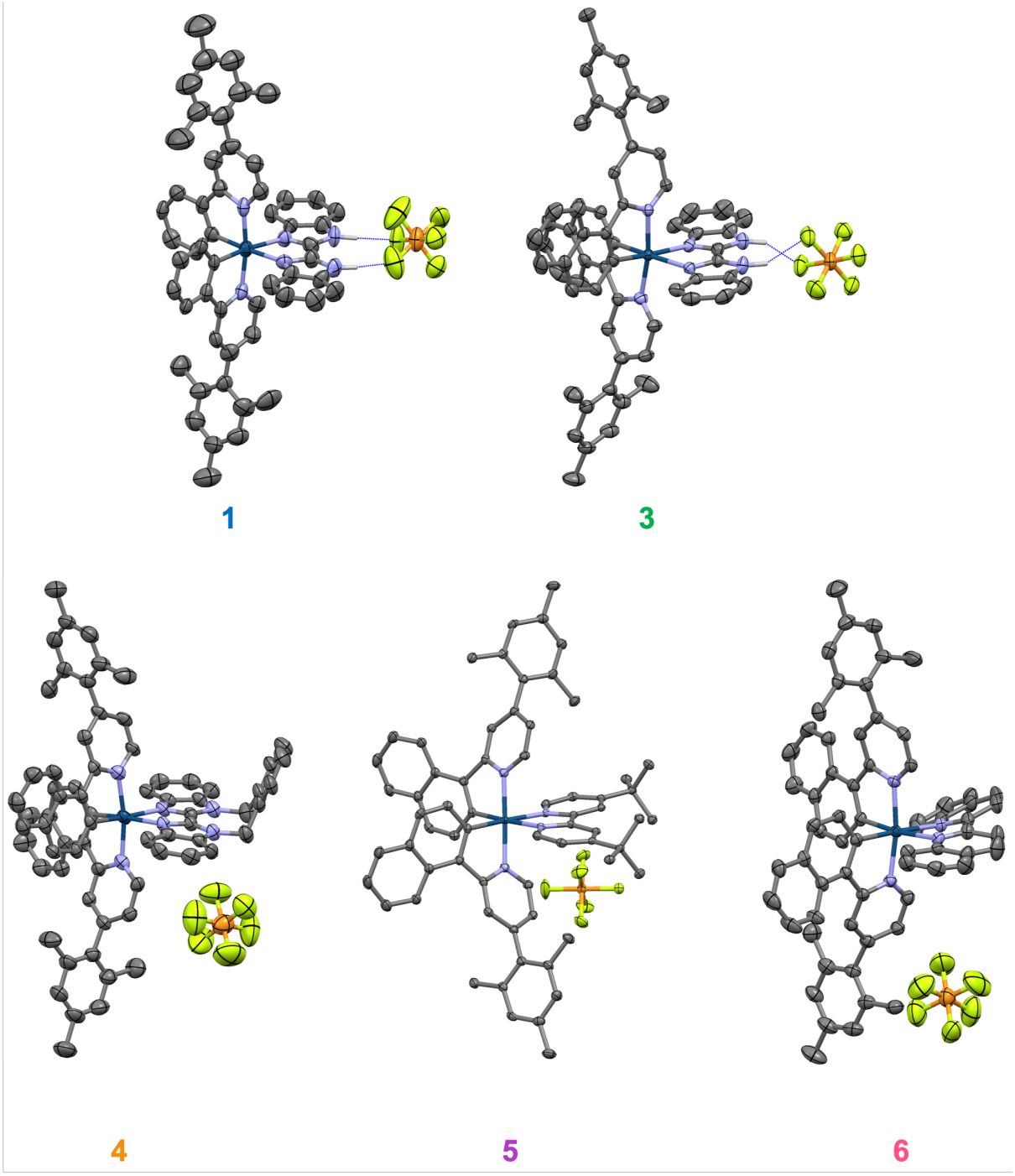

Figure **6**. X-ray crystal structures of complexes **1**, **3**, **4**, **5** and **6**. Solvent molecules and C-H hydrogen atoms have been removed for clarity. Counterions have been included to show hydrogen-bonding interactions observed for complexes **1** and **3**, where hydrogen bonding interactions are shown with dotted lines. Such interactions are not present in the crystal structures of **4**, **5** and **6**. Thermal ellipsoids are drawn at the 50 % probability level.

Electrochemical Properties:

Cyclic voltammetry (CV) was carried out on **1**–**6** in deaerated MeCN in order to assess electrochemical reversibility and the energies associated with the oxidation and reduction waves. The ferrocene/ferrocenium redox couple was used as the internal standard, and the redox potentials are reported *vs* SCE. The CV traces are shown in Figure **7** while relevant electrochemical data are given in Table **1**.

Table **1**. Relevant electrochemical data for complexes **1**–**6**.[a]

Complex	$E_{pa}^{(ox)}$ / V	$E_{pc}^{(ox)}$ / V	$\Delta E_p^{(ox)}$ / mV	$E_{pc}^{(red)}$ / V	$E_{pa}^{(red)}$ / V	$\Delta E_p^{(red)}$ / mV	ΔE / V [b]	E_{HOMO} / eV [c]	E_{LUMO} / eV [c]
1	1.33 [f]	1.21 [f]	120	-1.46 [e]	-	-	2.79	-5.53	-3.07
2	1.35 [f]	1.26 [f]	90	-1.41 [d]	-1.30 [d]	110	2.76	-5.57	-3.15
3	1.25 [d]	1.17 [d]	80	-1.41 [e]	-	-	2.66	-5.50	-3.11
4	1.18 [d]	1.09 [d]	90	-1.48 [d]	-1.38 [d]	100	2.66	-5.43	-3.07
5	1.26 [d]	1.16 [d]	100	-1.42 [d]	-1.33 [d]	90	2.42	-5.50	-3.13
6	1.11 [e]	-	-	-1.11 [d]	-1.03 [d]	80	2.22	-5.37	-3.49

[a] in MeCN at a scan rate of 100 mV s^{-1} with Fc/Fc^+ employed as an internal standard, and data reported *vs* SCE (Fc/Fc^+ = +0.38 V in MeCN).[27] [b] $\Delta E = E_{pa}^{(ox)} - E_{pc}^{(red)}$. [c] $E_{HOMO/LUMO} = -[E_{onset}^{ox/red}{}_{vs\ Fc/Fc+} + 4.8]$ eV.[28] [d] Reversible redox wave. [e] Irreversible redox wave. [f] Quasi-reversible redox wave.

The oxidation potentials of the complexes are sensitive to the nature of the C^N ligands. The first oxidation waves of **1** and **2** ($E_{pa}^{(ox)}$ = 1.33 V for **1** and 1.35 V for **2**), bearing Mesppy C^N ligands, come at similar potentials, and are quasi-reversible, respectively, while the oxidation waves in **3** and **4** are reversible and shifted cathodically ($E_{pa}^{(ox)}$ = 1.25 V for **3** and 1.18 V for **4**) due to the increased conjugation present in the Mesnpy C^N ligands. Our previously reported study on iridium complexes bearing functionalised biimidazole ligands showed that the oxidation potentials were sensitive to the nature of the biimidazole. For example, $[Ir(dFppy)_2(H_2biim)](PF_6)$ ($E_{1/2}^{(ox)}$ = 1.51 V) is anodically shifted compared to $[Ir(dFppy)_2(o\text{-}Xylbiim)](PF_6)$ ($E_{1/2}^{(ox)}$ = 1.44 V), and $[Ir(dFMesppy)_2(o\text{-}Xylbiim)](PF_6)$ ($E_{1/2}^{(ox)}$ = 1.37 V).[14h]

By contrast, the differences in oxidation potentials of the analogous complexes employing either H_2bibenz or *o*-Xylbibenz as the N^N ligand are much smaller (cf. **1** vs **2** and **3** vs **4**). When dtbubpy is used as the N^N ligand (**5**) there is almost no difference in the oxidation potential ($E_{pa}^{(ox)}$ = 1.26 V) compared to its mesityl-free analogue [Ir(npy)$_2$(dtbubpy)](PF$_6$), where npy is 2-(napthalen-1-yl)pyridine ($E_{1/2}^{(ox)}$ = 1.13 V).[29] These results are consistent with the solid-state crystal structure data where the methyl groups on the mesityl ring force it into a mutually orthogonal conformation with respect to the pyridine ring and thus electronically decouple it from the system.

Finally, in contrast to the complexes **1**–**5**, the oxidation of **6** is completely irreversible and is significantly cathodically shifted ($E_{pa}^{(ox)}$ = 1.11 V). The lower oxidation potential of **6** compared to [Ir(ppz)$_2$(biq)](PF$_6$) (where ppzH is 2-phenylpyrazole; $E_{1/2}^{(ox)}$ = 1.42 V),[22] and [Ir(ppy)$_2$(biq)](PF$_6$) ($E_{1/2}^{(ox)}$ = 1.24 V)[21] demonstrates the role played by the naphthyl ring in facilitating the oxidation process.

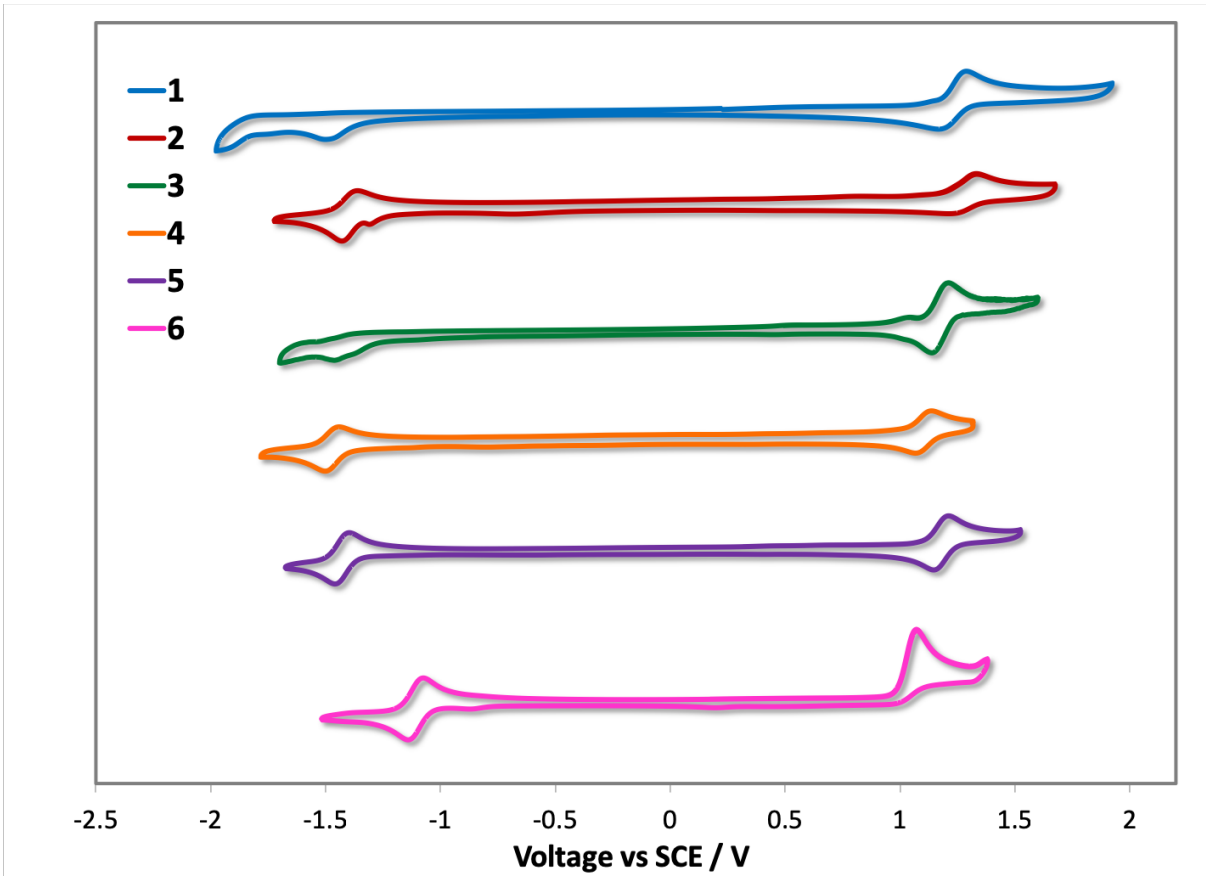

Figure **7**. CV traces of complexes **1**–**6** in deaerated MeCN solution, reported versus SCE (Fc/Fc^+ = 0.38 V in MeCN).[27] Scan rates are at 100 mV s^{-1} and scans are in the positive direction.

From these data, which are in line with the literature,[14h, 14k, 22, 30] and in accordance with the DFT computed ground state calculations (*vide infra*), the first oxidation waves of **1**–**6** can be ascribed to the Ir^{III}/Ir^{IV} redox couple, coupled with contribution from the cyclometalating arene of the C^N ligands. This latter contribution to the oxidation is evidenced by the modestly anodically shifted oxidation potentials of **1** and **2** ($E_{pa}^{(ox)}$ = 1.33–1.35 V), bearing Mesppy C^N ligands, compared to **3**–**6** ($E_{pa}^{(ox)}$ = 1.11–1.26 V) which have more conjugated Mesnpy C^N ligands.

The reduction potentials are much less sensitive to the nature of the C^N ligands, remaining largely unchanged for complexes **1**–**5** ($E_{pc}^{(red)}$ = -1.39 to -1.45 V for **1**–**5**). However, the reversibility of the reduction waves does appear to be ligand dependent. Complexes **1** and **3**, bearing the H_2bibenz N^N ligand, possess irreversible reduction waves, which suggest that the secondary amines are susceptible to electrochemical degradation processes upon reduction. Complexes **2** and **4**, bearing the alkylated *o*-Xylbibenz analogue, show reversible reduction waves, indicating that such unfavourable degradation processes observed for complexes **1** and **3** are blocked upon alkylation. The reduction of **5** is also reversible, which is a common feature of complexes bearing dtbubpy ligands. The reduction wave of **6** ($E_{pc}^{(red)}$ = -1.11 V) is also reversible and is significantly anodically shifted compared with **1**–**5**, as a result of the strong π-accepting character of the biq ligand. There are two important conclusions to draw from these results: 1) the reduction is predominantly an N^N-based process; a conclusion in line with the literature[14h, 14k, 22, 30] and DFT calculations (*vide infra*); 2) it was previously shown that the electron-releasing properties of H_2biim or *o*-Xylbiim N^N ligands destabilise the LUMO, and so complexes such as [Ir(dFMesppy)$_2$(*o*-Xylbiim)](PF$_6$) (ΔE = 3.36 V) have a much larger redox gap than analogous complexes bearing dtbubpy ligands, such as [Ir(dFMesppy)$_2$(dtbubpy)](PF$_6$) (ΔE = 2.95 V).[14h] However, in this work, this effect in complexes **1**–**4** is offset by the increased conjugation across the N^N ligand backbone seen in H_2bibenz and *o*-Xylbibenz. This second point is evidenced by studying the net redox gaps of complexes **3**–**5**, which are largely unchanged regardless of the N^N ligand (ΔE = 2.36–2.39 V for **3**–**5**). Although the oxidation potentials complexes **3** and **5** ($E_{pa}^{(ox)}$ = 1.25–1.26 V for **3** and **5**) are modestly anodically shifted compared to that of **4** ($E_{pa}^{(ox)}$ = 1.18 V), this is compensated for by a similar anodic shift in the reduction potentials of **3** ($E_{pc}^{(red)}$ = -1.41 V) and **5** ($E_{pc}^{(red)}$ = -1.42 V) compared to **4** ($E_{pc}^{(red)}$ = -1.48 V).

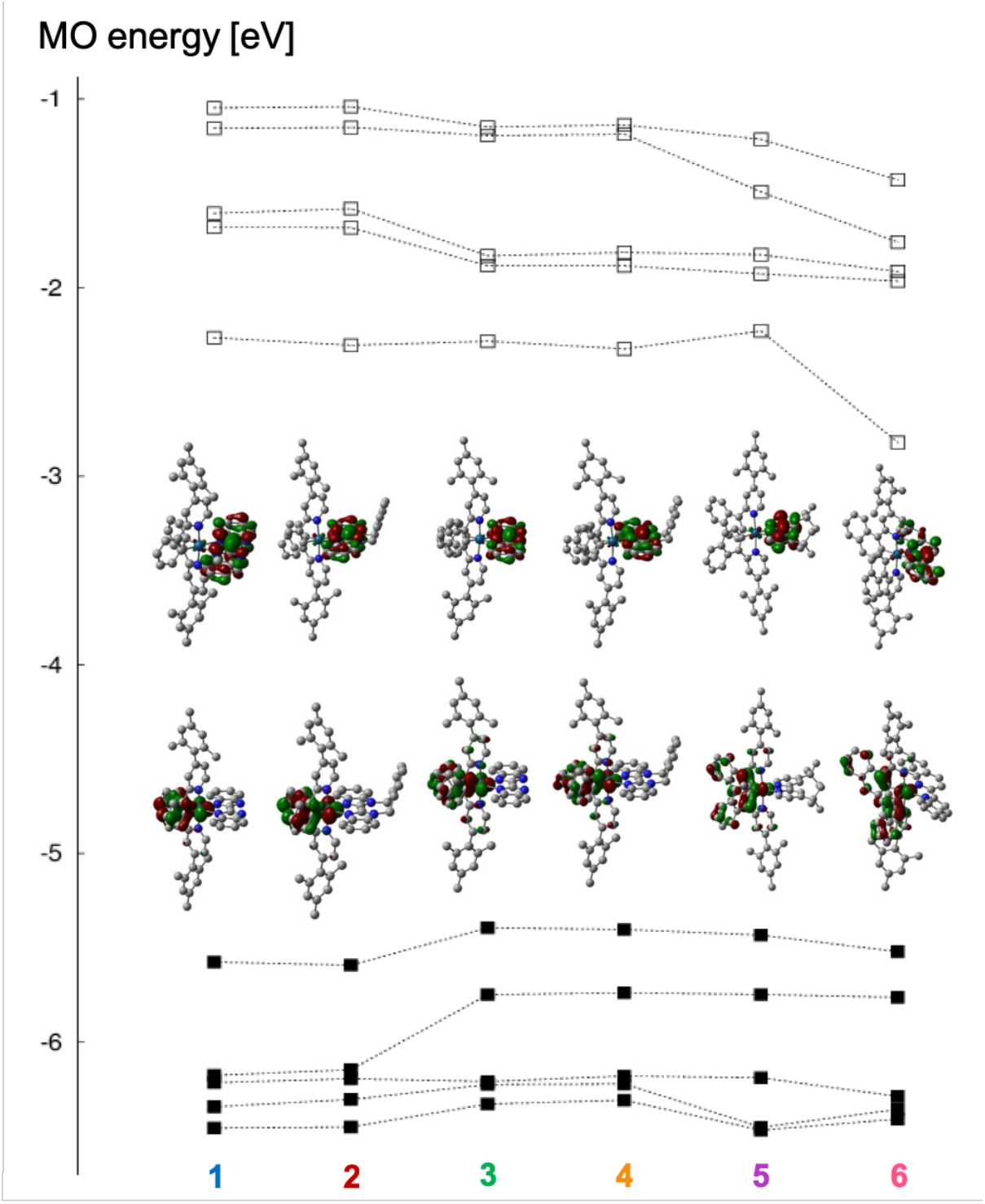

Figure **8**. Variation of the frontier MO energies (in eV) as a function of the ligand environment (singlet ground states, B3LYP level); the five highest occupied and the file lowest unoccupied orbital levels are shown. In the centre, plots of the HOMOs (below) and LUMOs (above) are included (H atoms omitted for clarity, isodensity value 0.04 a.u.).

Density functional theory (DFT) calculations (B3LYP on PBE0-optimized structures) largely corroborate the principal trends observed in the electrochemical data. A Kohn-Sham energy diagram of complexes **1**–**6**, as well as the electron density distribution plots for the HOMOs and LUMOs, is shown in Figure **8**. For each of the six complexes, the HOMO is comprised of almost equal contributions of iridium d-orbitals and cyclometalating aryl rings. The relative HOMO energies are predicted to be higher for complexes **3**–**6** than for **1** and **2** as a function of the increased conjugation of the Mesnpy C^N ligands. The principal theoretical deviation from the experimental data is that of the HOMO of complex **6**; from the CV trace this complex has the least positive oxidation potential ($E_{pa}^{(ox)}$ = 1.11 V) implying an oxidation process facilitated by a HOMO that is higher in energy than the other complexes in the series. By contrast, the DFT calculations predict a stabilisation in the HOMO energy of **6** relative to complexes **3**–**5**. The LUMO is localised almost exclusively on the N^N ligands albeit with a small metal-based contribution. There is predicted to be very little variation in the LUMO energies of complexes **1**–**5**, which supports the experimental assertions that the electronic behaviour of dtbubpy, H_2bibenz and *o*-Xylbibenz are largely indistinguishable. The large stabilization of the LUMO predicted for **6** corresponds well with the CV data. Even though there is no strict relation between MO energies and ionization potentials (IPs) or electron affinities (EAs) in DFT, the same trends are obtained in the actual computed vertical IPs and EAs (see Table S2 in the supporting information).

UV-Vis Absorption.

The UV-vis absorption spectra for **1**–**6** are shown in Figure **9** and the molar absorptivity data are reported in Table **2**. In the high-energy region of the spectrum (250–400 nm), π-π* transitions with high molar absorptivity dominate for all complexes. Among these, two distinct

sets of transitions can be identified: 250–300 nm and 300–400 nm. For complexes **1** and **2**, a single distinct higher energy π-π* transition (λ_{abs} = 263 nm for **1** and 270 nm for **2**) is observed, along with poorly resolved shoulders (λ_{abs} = 282 nm for **1** and 289 nm for **2**). For complexes **3** and **4**, similar transitions (λ_{abs} = 264 nm for **3** and 263 nm for **4**) are accompanied by well-resolved absorption bands (λ_{abs} = 295 nm for **3** and 291 nm for **4**) that are more highly absorptive and red-shifted compared to the corresponding shoulders present in **1** and **2**. These absorption bands are therefore assigned to π-π* transitions on the cyclometalating ligands. Higher absorptivities are also observed for complexes bearing *o*-Xylbibenz (**2** and **4**) compared to H_2bibenz (**1** and **3**), due to additional xylylene-centred π-π* transitions. The absorption spectrum of **5** shows a similar profile in the high energy region to those of **1**–**4** with a band at 266 nm, along with two shoulders at 285 and 294 nm. For **6**, the absorption spectrum in the high-energy region is dominated by a highly absorbing π-π* transition (λ_{abs} = 265 nm), obscuring the naphthyl-localised shoulder (λ_{abs} = 294 nm).

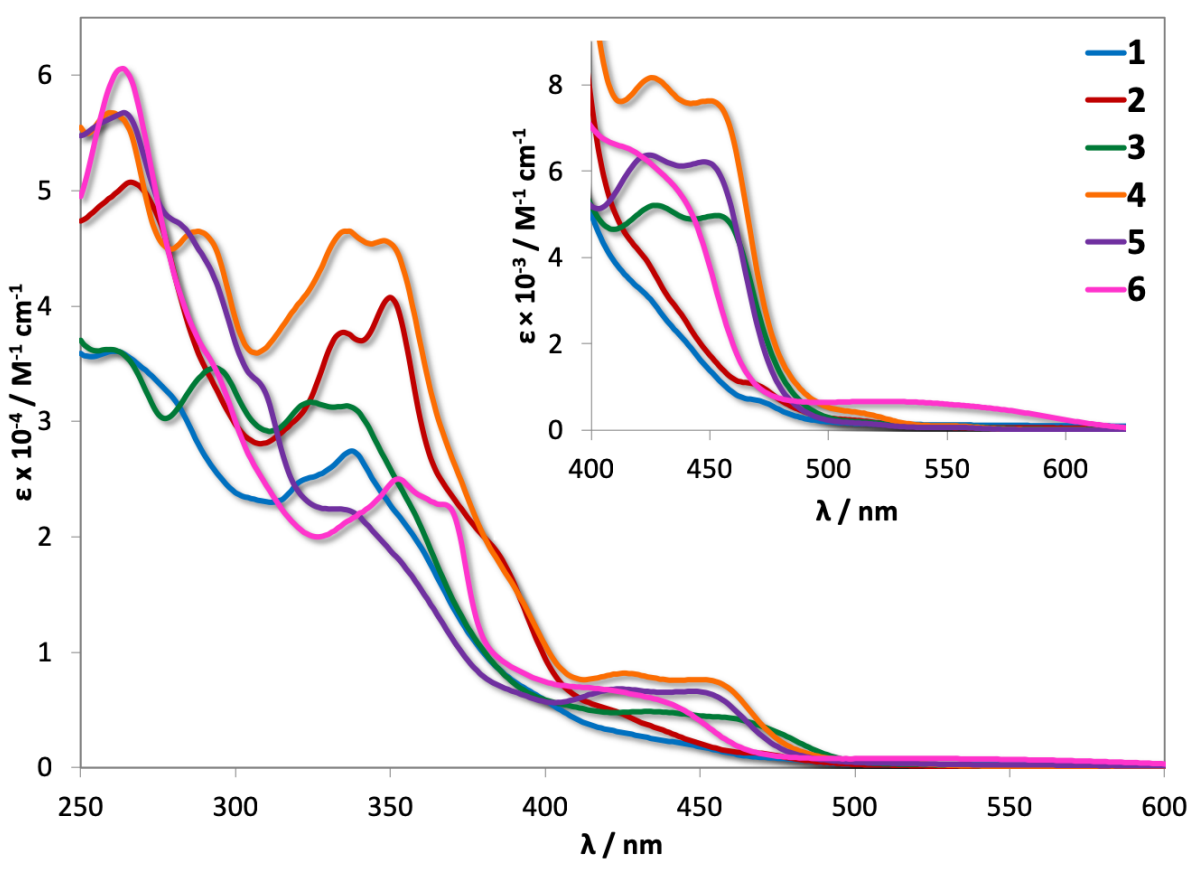

Figure **9**. UV-vis absorption spectra of complexes **1**–**6** in MeCN.

In the region between 300–400 nm, each complex possesses two well-defined, highly absorptive bands. The bands in this region are assigned to π-π* transitions involving the N^N ligand, evidenced by the near identical absorption maxima between **1** and **3** for this pair of bands (λ_{abs} = 322, 340 nm for **1** and 325, 339 nm for **3**); it is worth noting the moderately increased molar absorptivity observed for **3** compared to **1**. Similarly, these bands in **2** and **4** coincide (λ_{abs} = 335, 352 nm for **2** and 337, 351 nm for **4**) and are more strongly resolved, bathochromically-shifted, and significantly more absorptive than the corresponding bands in complexes **1** and **3**. The increased absorptivity observed for complexes **2** and **4** can be attributed to additional π-π* contributions from the xylylene bridge. The bands at 310 and 339 nm for **5** are hypsochromically shifted compared to those present in **1**–**4**, which are clustered between 322–339 and 340–361 nm, respectively. The pair of bands observed for **6** at 354 and 370 nm is the most red-shifted due to the greater π-accepting character of the biq ligand.

Table **2**. Absorption maxima and their corresponding molar absorptivities, as well as the optical gap for complexes **1**-**6**.[a]

Complex	λ_{abs} / nm [$\varepsilon \times 10^{-4}$ / M^{-1} cm^{-1}]	$E_{0\text{-}0}$ / nm
1	263 [3.60], 282(sh) [3.12], 322 [3.50], 340 [2.70], 361(sh) [1.86], 402 [0.55], 431 [0.27], 449 [0.18], 479 [0.07]	472
2	270 [5.01], 289(sh) [3.31], 335 [3.77], 352 [4.01], 386(sh) [1.80], 425 [0.46], 442 [0.28], 471 [0.12], 517 [0.02]	500
3	264 [3.60], 295 [3.45], 325 [3.17], 339 [3.10], 361(sh) [2.01], 436 [0.48], 463 [0.41], 517 [0.02], 559 [0.01]	538
4	263 [5.63], 291 [4.60], 319(sh) [3.97], 337 [4.65], 351 [4.52], 374(sh) [2.40], 391(sh) [1.52], 427 [0.82], 458 [0.71], 519 [0.04], 556 [0.01]	534
5	266 [5.64], 285(sh) [4.63], 294(sh) [4.19], 310 [3.23], 339 [2.20], 358(sh) [1.62], 391 [0.65], 422 [0.68], 454 [0.63], 517 [0.01], 555 [0.01]	540
6	265 [6.03], 294(sh) [3.43], 354 [2.49], 370 [2.22], 420 [0.68], 443(sh)[0.52], 539 [0.07]	550

[a] Measurements carried out in aerated MeCN. $E_{0\text{-}0}$ estimated from the intersection point of the absorption and emission spectra at 298 K in MeCN.

The absorption bands beyond 450 nm are assigned to mixed charge-transfer (CT) transitions on the basis of their lower absorptivity values. Surprisingly, these transitions are insensitive to the nature of the N^N ligands and are strongly affected by the nature of the C^N ligand, implying an unusual metal-to-C^N ligand (MLCT) transition, distinct from the typical metal-to-N^N ligand transitions generally associated with $[Ir(C^N)_2(N^N)]^+$ complexes.[31] Consider the spectra of complexes **1** and **2** featuring the Mesppy C^N ligand. Both these spectra show poorly resolved shoulders (λ_{abs} = 431 nm for **1** and 425 nm for **2**) and a low intensity absorption band (λ_{abs} = 449 nm for **1** and 442 nm for **2**). This is contrasted with the spectra of the Mesnpy complexes **3**–**5**, which exhibit red-shifted, highly absorptive, and well-resolved bands (λ_{abs} = 436, 463 nm for **3**, 427, 458 nm for **4** and 422, 454 nm for **5**). These spectra also contain a further red-shifted low intensity band at in the region of 555 nm (λ_{abs} = 559 nm for **3**, 556 nm for **4** and 555 nm for **5**). Thus, the presence of the naphthyl rings in **3**–**5** results in enhanced and red-shifted absorption bands in the near-UV region, compared to **1** and **2**. The absorption spectrum for **6** is distinct with only a single blue-shifted band at 443 nm. This, however, is coupled with a relatively strongly absorptive and broad band centred at 539 nm, tailing to ca. 640 nm that is attributed to spin-forbidden mixed CT transitions. Similar transitions are present for complexes **1**–**5**, but these are even less absorptive and have absorption onsets that are significantly blue-shifted (λ_{abs} < 585 nm for the onset of absorption of **1**–**5**). The general pattern of the absorption maxima in Table **2** is reasonably well reproduced, at least qualitatively, at the time-dependent DFT (TD-B3LYP) level (see Table S3 in the supporting information). Many dark states with zero or near-zero oscillator strength are predicted, but the transitions with significant oscillator strength tend to be close to the observed ones. In particular the trend in the observed λ_{max} values is well mirrored in the TD-B3LYP data, as is the strongly red-shifted spin-forbidden CT transition for complex **6** (computed at 602 nm, Table S3).

Emission Spectroscopy.

The emission spectra measured in deaerated MeCN for **1**–**6** are shown in Figure **10** and the photophysical data are summarized in Table **3**. TD-DFT calculations were undertaken to provide theoretical insight into the nature of the excited states and the computed spin density plots that describe the T_1 state are given in Figure **11**. Complex **1** is a green/yellow emitter (λ_{PL} = 500, 527 nm) with a narrow and somewhat structured emission profile. The short emission lifetime (τ_{PL} = 1.26 μs) coupled with a spin density distribution delocalized across the C^N and N^N ligands and the iridium centre, are indicative of a triplet excited state that is predominantly mixed ligand-to-ligand and metal-to-ligand charge transfer (^{3}MLCT/^{3}LLCT) in character. The structured emission profile suggests that there is also some ligand centred (^{3}LC) contribution to the excited state. The emission of $[Ir(ppy)_2(H_2bibenz)]PF_6$ has been reported previously in DCM and is red-shifted (Φ_{PL} = 534 nm) compared to **1** and reported as unstructured in nature.[32] This can be attributed to the more polar nature of the MeCN solvent, which can form hydrogen-bonds to the distal hydrogen atoms of the H_2bibenz ligand,[25a, 25c] polarizing this bond and increasing the effective electron density on the H_2bibenz ligand thereby leading to the blue-shift in the emission due to destabilisation of the ancillary ligand-based orbitals.

Table **3**. Relevant solution state photophysical data for complexes **1**–**6**.[a]

Complex	λ_{PL} / nm [b]	Φ_{PL} / % [c]	τ_{PL} / μs [d]	$k_r \times 10^{-5}$ / s^{-1}	$k_{nr} \times 10^{-5}$ / s^{-1}
1	500, 527	78	1.26	6.19	1.75
2	560, 580	89	1.83	4.86	0.60
3	585, 626	32	5.10	0.63	1.33
4	586, 623	44	7.65	0.58	0.73
5	580, 620	18	7.93	0.27	1.03
6	670	<1	-	-	-

[a] Measurements at 298 K in deaerated MeCN. [b] λ_{exc} = 420 nm. [c] $[Ru(bpy)_3]Cl_2$ used as the reference (Φ_{PL} = 4.0% in aerated water at 298 K).[33] [d] λ_{exc}: 375 nm.

Compared to **1**, the emission profile of complex **2** is significantly red-shifted (λ_{PL} = 560, 580 nm) and the excited state is moderately longer lived (τ_{PL} = 1.83μs). A similar trend is observed for the emission of complex [Ir(ppy)$_2$(dMebibenz)](PF$_6$) (where dMebibenz is 1,1'-dimethyl-2,2'-bibenzimidazole; λ_{PL} = 560, 580 nm) in DCM, wherein the complex with the alkylated bibenzimidazole ligand displays red-shifted emission compared to the protonated analogue [Ir(ppy)$_2$(H$_2$bibenz)]PF$_6$.[32] By contrast, the opposite trend was observed between the complexes [Ir(dFppy)$_2$(H$_2$biim)](PF$_6$) and [Ir(dFppy)$_2$(*o*-Xylbiim)](PF$_6$), where in the latter there was a small *blue-shift* in the emission as a function of a strongly ^{3}LC-based emission.[14e]

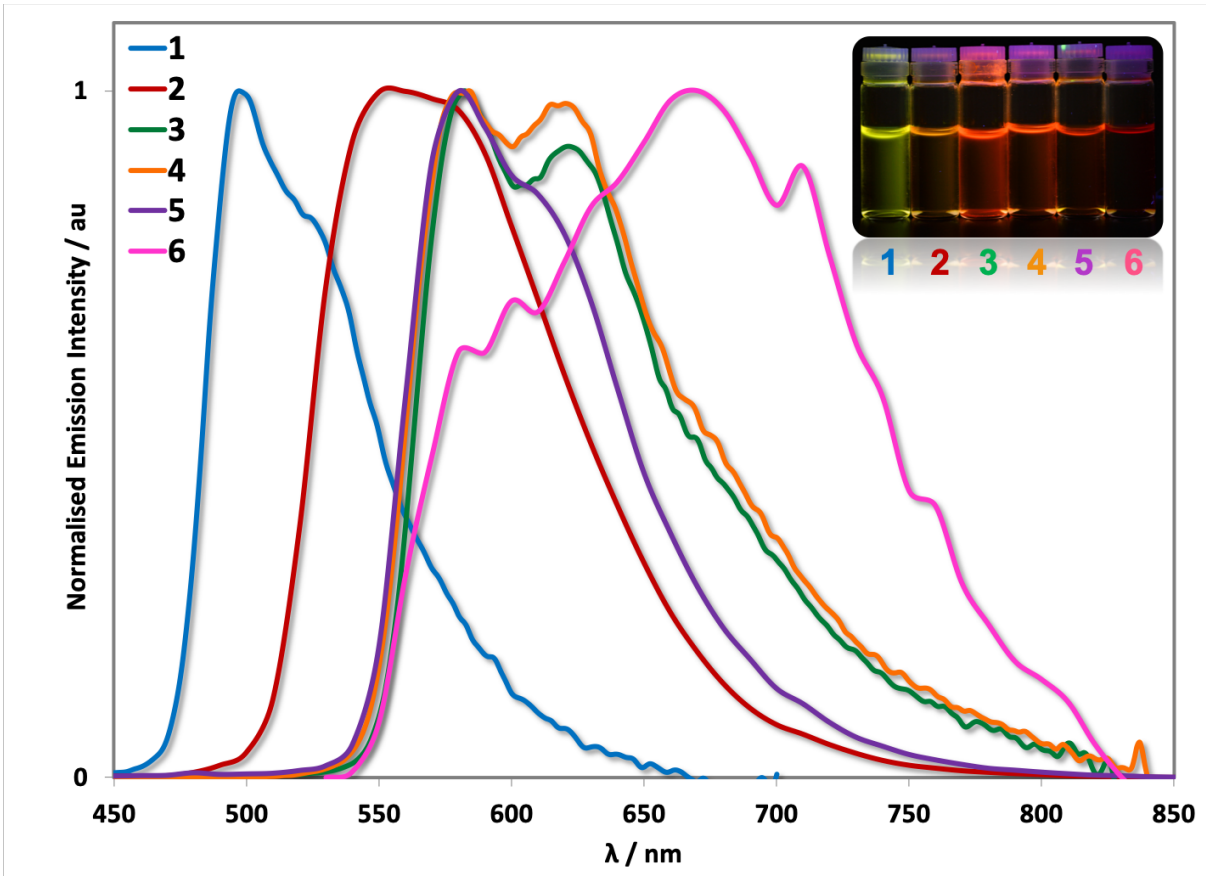

Figure **10**. Normalised emission spectra for **1**–**6** in deaerated MeCN solution. λ_{exc}: 420 nm. Inset: MeCN solutions of **1**–**6** (from left to right) illuminated under UV (365 nm) irradiation.

The differences observed in the emission spectra of complexes **1** and **2** are surprisingly not mirrored in the analogous comparison between **3** and **4**, which show virtually identical

emission spectra (λ_{PL} = 585, 626 nm for **3** and 586, 623 nm for **4**). This change in behaviour suggests that the presence of the naphthyl ring within the C^N ligands induces greater ^{3}LC character to the emissive triplet state, thereby making the emission of these complexes less sensitive to substitution on the ancillary ligand. The computed spin density distributions for **3** and **4** (Figure **11**) corroborate this assessment as they reveal a decidedly increased ^{3}LC character of the T_1 state of these two complexes compared to **1** and **2**. Likewise, complex **5** also emits from a ^{3}LC state, exhibiting a very similar emission profile to those of **3** and **4** (λ_{PL} = 580, 620 nm for **5**) and a spin density plot delocalised on the C^N ligand. These excited state characteristics mirror the ground state measurements carried out on **3**–**5**, wherein the electronic effects of the H_2bibenz, *o*-xylbibenz and dtbubpy are largely indistinct.

The ^{3}LC nature of the emission in complexes **3**–**5** appears to be typical of iridium complexes featuring cyclometalated naphthalene rings. For example, the archetypal $[Ir(C^N)_2(N^N)]^+$ complex, $[Ir(ppy)_2(dtbubpy)](PF_6)$ exhibits a broad and structured ^{3}MLCT/^{3}LLCT emission in solution (λ_{PL} = 591 nm; Φ_{PL} = 27%, τ_{PL} = 0.39 μs in MeCN).[34] However, incorporation of the naphthalene ring within the C^N ligand framework of the complex $[Ir(npy)_2(dtubpy)](PF_6)$ promoted a red-shifted and structured emission coupled with a long-lived excited state that are indicative of a ^{3}LC state (λ_{PL} = 590, 625 nm; Φ_{PL} = 1%, τ_{PL} = 8.3 μs in MeCN).[29]

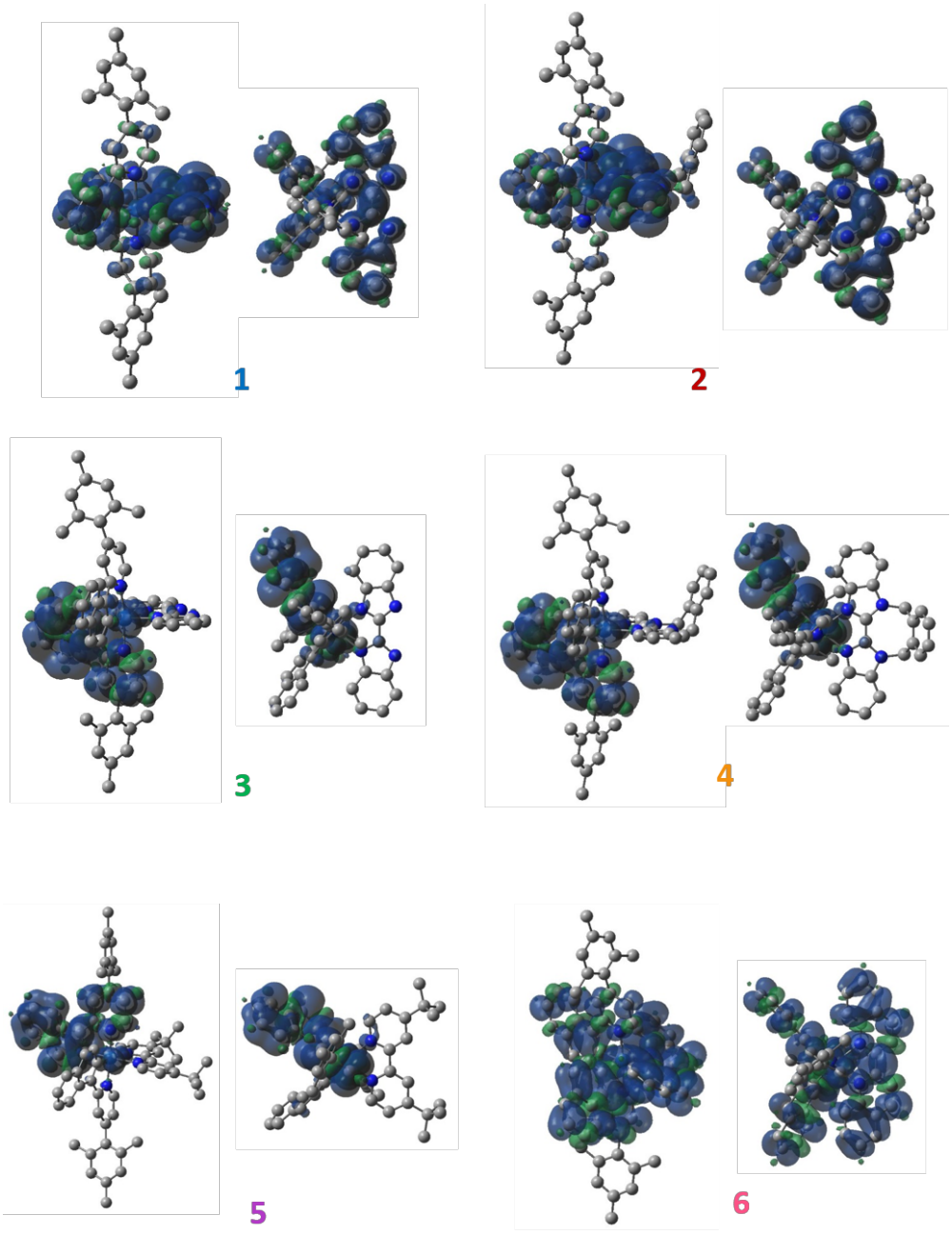

Figure **11**. Computed spin densities in the lowest triplet state (B3LYP level, H atoms omitted for clarity, isodensity value $4 \cdot 10^{-4}$ a.u.); two orientations are shown in each case, a side view (left of the labels) along the plane of the N^N ligand and a top view (right of the labels) down the axis of the mesityl rings of the C^N ligands.

Complex **6** exhibits the most red-shifted emission profile and is also the least emissive of the series. The spectrum is broad and noisy due to the low emission intensity of the complex. The

T_1 state is assigned as a mixed ^{3}LLCT and ^{3}MLCT state, which is mirrored in the spin density calculations carried out on **6**. The trend in the longest emission wavelengths parallels that of the computed vertical singlet-triplet splittings at the optimized structures of the triplets, although the resulting computed wavelengths (602 nm - 738 nm, see values in parentheses in the last column of Table S3) are largely overestimated with respect to experiment (527 nm - 670 nm, Table 3).

Complex **1** has a high Φ_{PL} and short lifetime (Φ_{PL} = 78%, τ_{PL} = 1.26 μs), which are in line with emission from a ^{3}CT state. Complex **1** thus exhibits the highest radiative rate constant among **1**–**6** (k_r = 6.19 × 10^5 s^{-1}). The higher Φ_{PL} of **1** compared to that reported for $[Ir(ppy)_2(H_2bibenz)](PF_6)$ (Φ_{PL} = 33% in DCM)[32] demonstrates the positive impact of the mesityl ring in inhibiting non-radiative decay processes. Alkylation with the *o*-xylene linker as in **2** results in an enhanced Φ_{PL} and longer emission lifetime values (Φ_{PL} = 89%, τ_{PL} = 1.83 μs). The rigidified design has a clear effect in this instance as the non-radiative decay rate of **2** (k_{nr} = 0.60 × 10^5 s^{-1}) is suppressed by an order of magnitude compared to that of **1** (k_{nr} = 1.75 × 10^5 s^{-1} for **2**), despite competing with the energy gap law as a function of more red-shifted emission. As expected, similar radiative rate constant values for **1** and **2** (k_r = 6.19 × 10^5 s^{-1} for **1** and 4.89 × 10^5 s^{-1} for **2**) show that this design feature impacts almost exclusively on non-radiative quenching processes. When comparing to the known $[Ir(Mesppy)_2(dtbubpy)](PF_6)$ (determined in MeCN),[18c] the emission was red-shifted, the excited state shorter-lived, and the Φ_{PL} lower (λ_{PL} = 592 nm, τ_{PL} = 0.64 μs, Φ_{PL} = 28%) in the known complex than for both complexes **1** and **2**. Thus, this is evidence for the merits of employing the H_2bibenz and *o*-Xylbibenz ligands for achieving efficient emission in solution.

When the Mesnpy C^N ligand is employed, two features become apparent: 1) the τ_{PL} values lengthen considerably as a consequence of the greater ^{3}LC character of the T_1 state; 2) the k_r values for complexes **3**–**5** are an order of magnitude smaller than for the Mesppy complexes, which is the result of both the ^{3}LC character in combination with the characteristic wavelength-dependent reduction in radiative rates due to the energy gap law. For example, the lifetime of **3** (τ_{PL} = 5.10 μs) is much longer than that of **1**, but the Φ_{PL} is lower (Φ_{PL} = 32%) resulting from a lower radiative rate constant ($k_r = 0.63 \times 10^5$ s^{-1}). These are classic features of ^{3}LC states, which phosphoresce via indirect spin-orbit coupling pathways that are less quantum mechanically probable than the direct pathways by which ^{3}CT states emit.[35] The analogous comparison can be made between complexes **2** (Φ_{PL} = 89%, τ_{PL} = 1.83 μs, $k_r = 4.86 \times 10^5$ s^{-1}) and **4** (Φ_{PL} = 44%, τ_{PL} = 7.65 μs, $k_r = 0.58 \times 10^5$ s^{-1}). As with **1** *vs* **2**, the merits of the xylylene bridge are evident, with a higher photoluminescence quantum yield observed for **4** versus **3**. Complex **5** is much less emissive (Φ_{PL} = 18%) than both complexes **3** and **4** due to a combination of a smaller radiative rate constant ($k_r = 0.27 \times 10^5$ s^{-1}) and a larger non-radiative rate constant ($k_{nr} = 1.03 \times 10^5$ s^{-1}). Nevertheless, **5** has an enhanced Φ_{PL} compared to [Ir(npy)$_2$(dtbubpy)](PF$_6$) (Φ_{PL} = 1% in MeCN),[29] illustrating the importance of the mesityl group in the Mesnpy C^N ligand towards inhibiting intermolecular quenching processes. Thus, the high Φ_{PL} values measured for **2** and **4** are a result of the ligand scaffolds working in concert to inhibit both *intra*molecular quenching processes (*o*-Xylbibenz), and *inter*molecular quenching processes (Mesppy/Mesnpy). Gratifyingly, we have been able to demonstrate that these principles can be applied across the visible spectrum.

To better elucidate the merits of employing our Mesnpy and *o*-Xylbibenz ligands in [Ir(C^N)$_2$(N^N)]$^+$ complexes, it is worth placing into context the photoluminescence quantum yield of **4** compared other cationic iridium(III) complexes with similar emission energies. We

recently reported an exhaustive analysis of $[Ir(C^N)_2(N^N)]^+$ used in LEECs,[6a] and among 33 complexes emitting in the orange-red (λ_{PL} > 599 nm) studied in this meta-analysis, only two had Φ_{PL} values higher than 20%, with the vast majority of these emitting with photoluminescence quantum yields less than 5%. Of the two complexes emitting with high Φ_{PL}, one complex, bearing a perylene diimide-functionalised (PDI) ancillary N^N ligand, emits with a higher photoluminescence quantum yield than seen for **4**, but this was attributed to a fluorescence mechanism localised directly on the PDI group (λ_{PL} = 619 nm; Φ_{PL} = 53%; τ_{PL} = 3.0 ns in MeCN).[36] The other complex was originally reported to emit with a Φ_{PL} of 53%,[37] but this value has since been revised to only 25% (λ_{PL} = 620 nm; Φ_{PL} = 25%; τ_{PL} = 0.39 μs in DCM).[38] Thus, it is clear from this evidence that employing ligands systematically designed to suppress k_{nr} is a fruitful strategy for enhancing the quantum yield.

Conclusions.

Building on our previous studies focussed on the rational design of highly emissive blue/green emitters, the present study showcases the versatility of our molecular design principles to rationally design red-emitting iridium complexes with high quantum yields, using conjugated C^N ligands modified with bulky mesityl substituents in concert with rigidified bibenzimidazole N^N ancillary ligands. We have shown that the Mesppy complex **1** emits in the yellow/green (λ_{PL} = 500, 527 nm) but with higher quantum yield (Φ_{PL} = 78%) than its previously reported mesityl-free analogue (Φ_{PL} = 33%). Replacing the H_2bibenz N^N ligand in **1** with the rigidified *o*-Xylbibenz ligand (**2**) red-shifts the emission (λ_{PL} = 560, 580 nm) and *enhances* the quantum yield further (Φ_{PL} = 89%). Further red-shifting is possible when the more conjugated Mesnpy C^N is adopted (λ_{PL} = 585–626 nm for **3**–**5** and 670 nm for **6**). Complexes **3**–**5** emit with virtually overlapping emission profiles, indicating emission from a similar excited state. However, mirroring **1** *vs* **2**, both **3** (H_2bibenz, Φ_{PL} = 32%) and especially

5 (dtbubpy, Φ_{PL} = 18%) are less emissive than **4** (*o*-Xylbibenz, Φ_{PL} = 44%). Complex **6**, with the biq N^N ligand, was found to be very poorly emissive. Comparing the quantum yield of **4** with other red-emitters studied in LEECs places it in the top three most emissive complexes reported to date. The investigation of these complexes in LEECs is ongoing, with a particular focus on the crucial role of film morphology in devices, which still requires optimization to enhance the device performance. We expect these results to positively inform the future design of luminescent iridium complexes for a variety of applications, including light-emitting devices.

Acknowledgements. EZ-C acknowledges the University of St Andrews for financial support. We thank Umicore AG for the gift of materials. We would like to thank the Engineering and Physical Sciences Research Council for financial support for E.Z-C. (EP/M02105X/1) and for the studentship of A.H. (EP/J500549/1, EP/K503162/1, EP/L505097/1). We thank the EPSRC UK National Mass Spectrometry Facility at Swansea University for analytical services. We also would like to thank EaStCHEM and the School of Chemistry for supporting the computing facilities maintained by Dr. H. Früchtl.

Supporting information. The following can be found in the Supporting Information: details of the relevant synthetic protocols for the ligands and complexes; characterisation of novel compounds synthesised herein; ^{1}H and ^{13}C NMR spectra; details of spectroscopic and electrochemical procedures; CIFs of the crystal structures, CCDC Nos. 1892241-1892246; details of theoretical calculations.

References

(1). E. Zysman-Colman, ed., *Iridium(III) in Optoelectronic and Photonics Applications*, John Wiley & Sons, Ltd, 2017.
(2). F. G. Gao and A. J. Bard, *J. Am. Chem. Soc.*, 2000, **122**, 7426-7427.
(3). (a) S. Bernhard, X. Gao, G. G. Malliaras and H. D. Abruña, *Adv. Mater.*, 2002, **14**, 433; (b) D. A. Ross, P. A. Scattergood, A. Babaei, A. Pertegas, H. J. Bolink and P. I. Elliott, *Dalton Trans*, 2016, **45**, 7748-7757.
(4). A. F. Henwood and E. Zysman-Colman, *Chem. Commun.*, 2017, **53**, 807-826.
(5). Y. Im, S. Y. Byun, J. H. Kim, D. R. Lee, C. S. Oh, K. S. Yook and J. Y. Lee, *Adv. Funct. Mater.*, 2017, **27**.
(6). (a) A. F. Henwood and E. Zysman-Colman, in *Iridium(III) in Optoelectronic and Photonics Applications*, John Wiley & Sons, Ltd, 2017, pp. 275-357; (b) A. F. Henwood and E. Zysman-Colman, *Top. Curr. Chem.*, 2016, **374**, 36; (c) C. E. Housecroft and E. C. Constable, *Coord. Chem. Rev.*, 2017, **350**, 155-177; (d) S. Tang and L. Edman, *Top Curr Chem (J)*, 2016, **374**, 40; (e) R. D. Costa, E. Ortí, H. J. Bolink, F. Monti, G. Accorsi and N. Armaroli, *Angew. Chem. Int. Ed.*, 2012, **51**, 8178-8211; (f) E. Fresta and R. D. Costa, *J. Mater. Chem. C*, 2017, **5**, 5643-5675; (g) D. Ma, T. Tsuboi, Y. Qiu and L. Duan, *Adv Mater*, 2017, **29**, 1603253.
(7). (a) J. V. Caspar, E. M. Kober, B. P. Sullivan and T. J. Meyer, *J. Am. Chem. Soc.*, 1982, **104**, 630-632; (b) S. H. Lin, *J. Chem. Phys.*, 1966, **44**, 3759-3767; (c) M. Bixon and J. Jortner, *J. Chem. Phys.*, 1968, **48**, 715-726; (d) K. F. Freed and J. Jortner, *J. Chem. Phys.*, 1970, **52**, 6272-6291; (e) J. Jortner, *Mol. Phys.*, 1970, **18**, 145-164.
(8). P.-N. Lai, C. H. Brysacz, M. K. Alam, N. A. Ayoub, T. G. Gray, J. Bao and T. S. Teets, *J. Am. Chem. Soc.*, 2018, **140**, 10198-10207.
(9). H. Yersin, *Highly Efficient OLEDs with Phosphorescent Materials*, Wiley-VCH, Weinheim, 2008.
(10). J. V. Caspar and T. J. Meyer, *J. Phys. Chem.*, 1983, **87**, 952-957.
(11). (a) D. H. Kim, N. S. Cho, H.-Y. Oh, J. H. Yang, W. S. Jeon, J. S. Park, M. C. Suh and J. H. Kwon, *Adv. Mater.*, 2011, **23**, 2721-2726; (b) J. Zhang, L. Zhou, H. A. Al-Attar, K. Shao, L. Wang, D. Zhu, Z. Su, M. R. Bryce and A. P. Monkman, *Adv. Funct. Mater.*, 2013, **23**, 4667-4677.
(12). (a) C. Jin, R. Guan, J. Wu, B. Yuan, L. Wang, J. Huang, H. Wang, L. Ji and H. Chao, *Chem. Commun.*, 2017, **53**, 10374-10377; (b) Y. Liu, P. Zhang, X. Fang, G. Wu, S. Chen, Z. Zhang, H. Chao, W. Tan and L. Xu, *Dalton Trans.*, 2017, **46**, 4777-4785.
(13). (a) T. Huang, Q. Yu, S. Liu, W. Huang and Q. Zhao, *Dalton Trans.*, 2018, **47**, 7628-7633; (b) J. S. Nam, M.-G. Kang, J. Kang, S.-Y. Park, S. J. C. Lee, H.-T. Kim, J. K. Seo, O.-H. Kwon, M. H. Lim, H.-W. Rhee and T.-H. Kwon, *J. Am. Chem. Soc.*, 2016, **138**, 10968-10977.
(14). (a) S. Ladouceur, D. Fortin and E. Zysman-Colman, *Inorg. Chem.*, 2011, **50**, 11514-11526; (b) S. Ladouceur, K. N. Swanick, S. Gallagher-Duval, Z. Ding and E. Zysman-Colman, *Eur. J. Inorg. Chem.*, 2013, **2013**, 5329-5343; (c) L. Donato, P. Abel and E. Zysman-Colman, *Dalton Trans.*, 2013, **42**, 8402-8412; (d) S. Evariste, M. Sandroni, T. W. Rees, C. Roldan-Carmona, L. Gil-Escrig, H. J. Bolink, E. Baranoff and E. Zysman-Colman, *J. Mater. Chem. C*, 2014, **2**, 5793-5804; (e) A. F. Henwood, S. Evariste, A. M. Z. Slawin and E. Zysman-Colman, *Faraday Discuss.*, 2014, **174**, 165-182; (f) K. Hasan, A. K. Pal, T. Auvray, E. Zysman-Colman and G. S. Hanan, *Chem. Commun.*, 2015, **51**, 14060-14063; (g) N. M. Shavaleev, G. Xie, S. Varghese, D. B. Cordes, A. M. Z. Slawin, C. Momblona, E. Ortí, H. J. Bolink, I. D. W. Samuel and E. Zysman-Colman, *Inorg. Chem.*, 2015, **54**, 5907-5914; (h) A. F. Henwood, A. K. Bansal, D. B. Cordes, A. M. Z. Slawin, I. D. W. Samuel and E. Zysman-Colman, *J. Mater. Chem. C*, 2016, **4**, 3726-3737; (i) M. T. Sajjad, N. Sharma, A. K. Pal, K. Hasan, G. Xie, L. S. Kölln, G. S. Hanan, I. D. W. Samuel and E. Zysman-Colman, *J. Mater. Chem. C*, 2016, **4**, 8939-8946; (j) A. F. Henwood, A. K. Pal, D. B. Cordes, A. M. Z. Slawin, T. W. Rees, C. Momblona, A. Babaei, A. Pertegas, E. Orti, H. J. Bolink, E. Baranoff and E. Zysman-Colman, *J. Mater. Chem.*

C, 2017, **5**, 9638-9650; (k) A. K. Pal, A. F. Henwood, D. B. Cordes, A. M. Z. Slawin, I. D. W. Samuel and E. Zysman-Colman, *Inorg Chem*, 2017, **56**, 7533-7544; (l) J. M. Fernandez-Hernandez, S. Ladouceur, Y. Shen, A. Iordache, X. Wang, L. Donato, S. Gallagher-Duval, M. de Anda Villa, J. D. Slinker, L. De Cola and E. Zysman-Colman, *J. Mater. Chem. C*, 2013, **1**, 7440-7452; (m) D. Rota Martir, A. K. Bansal, V. Di Mascio, D. B. Cordes, A. F. Henwood, A. M. Z. Slawin, P. C. J. Kamer, L. Martinez-Sarti, A. Pertegas, H. J. Bolink, I. D. W. Samuel and E. Zysman-Colman, *Inorg. Chem. Frontiers*, 2016, **3**, 218-235.
(15). (a) C. Hierlinger, D. B. Cordes, A. M. Z. Slawin, A. Colombo, C. Dragonetti, S. Righetto, D. Roberto, D. Jacquemin, E. Zysman-Colman and V. Guerchais, *Dalton Trans*, 2018, **47**, 8292-8300; (b) K. Hasan, A. K. Bansal, I. D. W. Samuel, C. Roldán-Carmona, H. J. Bolink and E. Zysman-Colman, *Sci. Rep.*, 2015, **5**, 12325.
(16). A. K. Pal, D. B. Cordes, A. M. Z. Slawin, C. Momblona, A. Pertegas, E. Orti, H. J. Bolink and E. Zysman-Colman, *RSC Advances*, 2017, **7**, 31833-31837.
(17). (a) A. M. Bünzli, H. J. Bolink, E. C. Constable, C. E. Housecroft, M. Neuburger, E. Ortí, A. Pertegás and J. A. Zampese, *Eur. J. Inorg. Chem.*, 2012, **2012**, 3780-3788; (b) E. C. Constable, C. E. Housecroft, P. Kopecky, C. J. Martin, I. A. Wright, J. A. Zampese, H. J. Bolink and A. Pertegas, *Dalton Trans*, 2013, **42**, 8086-8103.
(18). (a) D. R. Martir, C. Momblona, A. Pertegás, D. B. Cordes, A. M. Z. Slawin, H. J. Bolink and E. Zysman-Colman, *ACS Appl. Mater. Interfaces*, 2016, **8**, 33907-33915; (b) D. Rota Martir, G. J. Hedley, D. B. Cordes, A. M. Z. Slawin, D. Escudero, D. Jacquemin, T. Kosikova, D. Philp, D. M. Dawson, S. E. Ashbrook, I. D. W. Samuel and E. Zysman-Colman, *Dalton Trans.*, 2016, **45**, 17195-17205; (c) C. Hierlinger, E. Trzop, L. Toupet, J. Ávila, M.-G. La-Placa, H. J. Bolink, V. Guerchais and E. Zysman-Colman, *J. Mater. Chem. C*, 2018, **6**, 6385-6397; (d) H. Benjamin, M. A. Fox, A. S. Batsanov, H. A. Al-Attar, C. Li, Z. Ren, A. P. Monkman and M. R. Bryce, *Dalton Trans*, 2017, **46**, 10996-11007.
(19). (a) L. He, L. Duan, J. Qiao, G. Dong, L. Wang and Y. Qiu, *Chem. Mater.*, 2010, **22**, 3535-3542; (b) S. Jo and Y. S. Choe, *Molecular Crystals and Liquid Crystals*, 2017, **654**, 221-233.
(20). V. N. Kozhevnikov, Y. Zheng, M. Clough, H. A. Al-Attar, G. C. Griffiths, K. Abdullah, S. Raisys, V. Jankus, M. R. Bryce and A. P. Monkman, *Chem. Mater.*, 2013, **25**, 2352-2358.
(21). H.-C. Su, H.-F. Chen, F.-C. Fang, C.-C. Liu, C.-C. Wu, K.-T. Wong, Y.-H. Liu and S.-M. Peng, *J. Am. Chem. Soc.*, 2008, **130**, 3413-3419.
(22). A. B. Tamayo, S. Garon, T. Sajoto, P. I. Djurovich, I. M. Tsyba, R. Bau and M. E. Thompson, *Inorg. Chem.*, 2005, **44**, 8723-8732.
(23). (a) Y. Yasui, D. K. Frantz and J. S. Siegel, *Org. Lett.*, 2006, **8**, 4989-4992; (b) D. K. Frantz, A. Linden, K. K. Baldridge and J. S. Siegel, *J. Am. Chem. Soc.*, 2012, **134**, 1528-1535.
(24). M. Nonoyama, *Bull. Chem. Soc. Jpn.*, 1974, **47**, 767-768.
(25). (a) J. C. Freys, G. Bernardinelli and O. S. Wenger, *Chem. Commun.*, 2008, 4267-4269; (b) K. Heussner, K. Peuntinger, N. Rockstroh, L. C. Nye, I. Ivanovic-Burmazovic, S. Rau and C. Streb, *Chem. Commun.*, 2011, **47**, 6852-6854; (c) S. Derossi, H. Adams and M. D. Ward, *Dalton Trans*, 2007, 33-36.
(26). (a) Y. Ma, J. Yang, S. Liu, H. Xia, P. She, R. Jiang and Q. Zhao, *Adv. Optical Mater.*, 2017, **5**; (b) Y. Cui, Y.-L. Niu, M.-L. Cao, K. Wang, H.-J. Mo, Y.-R. Zhong and B.-H. Ye, *Inorg. Chem.*, 2008, **47**, 5616-5624.
(27). V. V. Pavlishchuk and A. W. Addison, *Inorg. Chim. Acta*, 2000, **298**, 97-102.
(28). C. M. Cardona, W. Li, A. E. Kaifer, D. Stockdale and G. C. Bazan, *Adv. Mater.*, 2011, **23**, 2367-2371.
(29). S. Medina-Rodriguez, S. A. Denisov, Y. Cudre, L. Male, M. Marin-Suarez, A. Fernandez-Gutierrez, J. F. Fernandez-Sanchez, A. Tron, G. Jonusauskas, N. D. McClenaghan and E. Baranoff, *Analyst*, 2016, **141**, 3090-3097.

(30). Q. Zhao, S. Liu, M. Shi, C. Wang, M. Yu, L. Li, F. Li, T. Yi and C. Huang, *Inorg. Chem.*, 2006, **45**, 6152-6160.
(31). (a) S. Ladouceur, D. Fortin and E. Zysman-Colman, *Inorg. Chem.*, 2010, **49**, 5625-5641. and references cited therein; (b) S. Ladouceur and E. Zysman-Colman, *Eur. J. Inorg. Chem.*, 2013, **2013**, 2985-3007.
(32). L. K. McKenzie, I. V. Sazanovich, E. Baggaley, M. Bonneau, V. Guerchais, J. A. Williams, J. A. Weinstein and H. E. Bryant, *Chemistry*, 2017, **23**, 234-238.
(33). W. H. Melhuish, *J. Phys. Chem.*, 1961, **65**, 229-235.
(34). For examples see: S. Ladouceur, D. Fortin and E. Zysman-Colman, *Inorg. Chem.*, 2011, **50**, 11514-11526.
(35). H. Yersin, A. F. Rausch, R. Czerwieniec, T. Hofbeck and T. Fischer, *Coord. Chem. Rev.*, 2011, **255**, 2622-2652.
(36). R. D. Costa, F. J. Cespedes-Guirao, E. Orti, H. J. Bolink, J. Gierschner, F. Fernandez-Lazaro and A. Sastre-Santos, *Chem. Commun.*, 2009, 3886-3888.
(37). H. J. Bolink, L. Cappelli, E. Coronado, M. Grätzel, E. Orti, R. D. Costa, P. M. Viruela and M. K. Nazeeruddin, *J. Am. Chem. Soc.*, 2006, **128**, 14786-14787.
(38). K. J. Suhr, L. D. Bastatas, Y. Shen, L. A. Mitchell, G. A. Frazier, D. W. Taylor, J. D. Slinker and B. J. Holliday, *Dalton Trans*, 2016, **45**, 17807-17823.

TOC Graphic